Surface & Coatings Technology 518 (2025) 132883

Contents lists available at ScienceDirect

Surface & Coatings Technology

journal homepage: www.elsevier.com/locate/surfcoat

Carbazole-functionalized nanocomposite fibers for sensitive alcohol vapor detection☆

Tz-Feng Lin [a,1], Yin-Hsuan Chang [b,1], Ting-Hung Hsieh [b], Shu-Chi Lu [b], Ting-Han Lin [c], Hao-Yun Yu [b], Ming-Chung Wu [b,c,d,e,*]

[a] Department of Chemical Engineering, National United University, Miaoli, 360302, Taiwan
[b] Department of Chemical and Materials Engineering, College of Engineering, Chang Gung University, Taoyuan, 333323, Taiwan
[c] Center for Sustainability and Energy Technologies, Chang Gung University, Taoyuan, 333323, Taiwan
[d] Division of Neonatology, Department of Pediatrics, Chang Gung Memorial Hospital, Linkou, Taoyuan, 333423, Taiwan
[e] Department of Materials Engineering, Ming Chi University of Technology, New Taipei City, 243303, Taiwan

ARTICLE INFO

Keywords:
Electrospinning
Alcohol gas sensing
Carbazole
Hydrophobic nanofibers
Volatile organic compounds detection

ABSTRACT

The detection of alcohol vapors is essential for industrial safety, environmental monitoring, and public health, as excessive exposure can pose serious hazards. Recent advances in gas sensing technologies, such as metal oxide semiconductors, conducting polymers, and surface acoustic wave sensors, have shown promise for detecting volatile organic compounds (VOCs), but challenges such as slow response time, poor selectivity, and humidity interference remain unresolved. Optical sensing platforms, especially those based on nanofibers, offer a promising alternative for achieving real-time, label-free detection in ambient conditions. In this work, poly(methyl methacrylate) (PMMA) was selected as the sensing matrix due to its excellent optical transparency, mechanical flexibility, and compatibility with molecular dopants. Carbazole-based compounds are designed by grafting two 4,4′-dimethoxy-diphenylamine (DPA) and functionalize with alkyl chains of varying lengths: 1-bromocetane (C16), and was identified as the optimal structure (DPA-C16). Silver nanoparticles (Ag NPs) were incorporated to enhance sensing performance via surface plasmon resonance (SPR). DPA-C16 was electrospun with PMMA and Ag nanoparticles to form nanofiber-based optical sensing films for alcohol detection. This study highlights the role of carbazole-based DPA-C16 in enhancing the morphology and performance of electrospun nanofibers for alcohol gas sensing. DPA-C16 significantly improves hydrophobicity, effectively reducing moisture interference, and thereby enhancing sensor stability in humid conditions. Optimized electrospun fiber materials exhibit rapid response times of less than one minute and high sensitivity with a detection limit of 50 ppm for methanol, ethanol, and isopropanol. The developed material demonstrates efficient and highly selective gas sensing capabilities, making it a strong candidate for industrial detection, environmental monitoring, and safety applications.

1. Introduction

Methanol, ethanol, and isopropanol are versatile volatile organic compounds (VOCs) widely employed in applications ranging from household cleaning and disinfection to industrial manufacturing and laboratory processes. While their utility is undeniable, improper handling or excessive accumulation of these alcohol-based compounds can pose severe risks to human health, safety, and the environment. [1–5] As highly flammable substances, they present a significant risk of fire and explosion, particularly in industrial and laboratory settings where large quantities are stored or used. Implementing accurate sensing systems is crucial to detecting leaks or unsafe vapor concentrations early, enabling timely interventions to mitigate hazards and ensure safer working environments.

Electrospinning is a versatile and efficient technique for fabricating high-performance sensing materials due to its ability to produce ultrafine fibers with unique structural properties. [6–9] Poly(methyl methacrylate) (PMMA) is a versatile and widely used amorphous

☆ This article is part of a Special issue entitled: 'SDSE 2024' published in Surface & Coatings Technology.

* Corresponding author at: Department of Chemical and Materials Engineering, College of Engineering, Chang Gung University, Taoyuan, 333323, Taiwan.
E-mail address: mingchungwu@cgu.edu.tw (M.-C. Wu).

[1] These authors contributed equally to this work.

https://doi.org/10.1016/j.surfcoat.2025.132883
Received 31 January 2025; Received in revised form 15 October 2025; Accepted 30 October 2025
Available online 1 November 2025

thermoplastic that has gained prominence in various industries due to its high strength, high stiffness, optical transparency, and good processability has led to its widespread application. [10–13] At present, the research mainly improves their properties by improving their morphology or further exploring their structural components through composite. For instance, the integration of conducting polymers such as polyaniline (PANI) into PMMA fibers has been proven to show good miscibility between two polymers and shown to significantly improve sensing capabilities. [14–16] PMMA/reduced graphene oxide (rGO) demonstrates high sensitivity towards NH_3. The incorporation of rGO leads to a significant increase in the surface roughness of PMMA, indicating successful surface modification. This enhancement is beneficial for improving interactions with NH_3 molecules. [12] Tailoring the optical and electrical properties of PMMA through the incorporation of noble metals such as Cu, Ag, and Au has been extensively studied. These metals exhibit strong surface plasmon resonance (SPR), a phenomenon arising from the collective oscillation of valence electrons. This property can be finely tuned for various applications, including sensing technologies. Noble metal nanoparticles embedded in PMMA can create "hot spots" that enhance the Raman signal of molecules near the surface. This sensitivity makes noble metals-PMMA composites ideal for detecting low concentrations of analytes, such as pollutants or biomolecules, which is crucial in environmental monitoring and medical diagnostics. [17–21]

Conductive polymers are vital in sensor design due to their electroactivity, flexibility, and multifunctionality. [22–25] Carbazole-based sensors are particularly notable for their excellent chemical stability, high fluorescence quantum yield, and strong π-conjugated structures, which enable efficient charge transfer. [26–30] Upon binding with Fe^{3+}, an intramolecular charge transfer process induces significant fluorescence quenching, enabling highly sensitive detection with a detection limit as low as 12.22×10^{-9} M. [31] An amperometric ethanol biosensor, using the novel monomer 9-methyl-9H-carbazole-3-carboxaldehyde hydrazone (MCCH), was developed. Electrochemical polymerization of MCCH onto graphite electrodes formed a conductive polymer film for enzyme immobilization. The sensor demonstrated high selectivity for ethanol over other alcohols, such as methanol and isopropanol. [32]

This study aims to develop highly selective and sensitive fiber-based alcohol sensors using carbazole-based compounds. Carbazole-based compounds are designed by grafting two 4,4′-dimethoxy-diphenylamine (DPA) and functionalized with alkyl chains, 1-bromocetane (C16). The DPA-C16 compound is further combined with silver and PMMA through electrospinning to fabricate a fiber-based alcohol sensing material. Gas sensing experiments are conducted using methanol, ethanol, and isopropanol to evaluate the detection limits and overall sensing performance. The DPA-C16/Ag/PMMA fibers achieves a rapid response time of less than 1 min and a detection limit of 50 ppm for alcohol vapors. The sensing mechanism of the DPA-C16/Ag/PMMA fibers is systematically analyzed and summarized. The results demonstrate that DPA-C16/Ag/PMMA fibers are efficient and selective gas-sensing materials with significant potential for industrial, environmental, and safety applications, and offer scope for further optimization and expansion into the detection of VOCs.

2. Experimental section

2.1. Synthesis of Ag nanoparticles

Silver nanoparticles (Ag NPs) were prepared through a solution-based chemical reduction method. Silver nitrate ($AgNO_3$, >99.5 %, Sigma−Aldrich) was used as a precursor, while oleylamine ($C_{18}H_{37}N$, >98 %, Sigma−Aldrich) acted as the reducing and stabilizing agent. In a typical synthesis, 0.6 mmol of $AgNO_3$ and 6.0 mmol of oleylamine were dissolved in 50.0 ml of chlorobenzene (C_6H_5Cl, >99 %, Acros) within a four-necked reaction flask. The solution was heated to 120 °C and maintained at this temperature for 1 h under continuous stirring in a nitrogen atmosphere. Following the reaction, the mixture was cooled to room temperature, and the resulting Ag NPs were dispersed in chlorobenzene for subsequent applications in material fabrication.

2.2. Synthesis of carbazole-based compounds

Carbazole-based compounds were designed with two 4,4′-dimethoxy-diphenylamine (DPA) moieties and grafted with alkyl chains, 1-bromocetane (C16). The as-formed DPA-C16 structures were studied for their VOC detection capabilities. According to the synthetic routes that have been published, 2,7-dibromocarbazole (1.39 g, 4.2 mmol) and K_2CO_3 (1.10 g, 8.0 mmol) were mixed together in a flask bottle containing 25 ml of dimethylformamide (DMF, C_3H_7NO, >99.5 %, Fisher Scientific). After the excess addition of C16 in 2 ml, the solution color was observed from transparent to pale yellow. It shows the protonation and substitution of the 2,7-dibromocarbazole molecular. The reaction temperature and time are 110 °C and 16 h, respectively. The crude product was extracted from ethyl acetate and deionized water three times. Then, the target product Br-C16 was separated from column chromatography, resulting in a white powder with a yield of 90 % above. Subsequently, the bromo sites of Br-C16 were respectively replaced by the 4,4′-dimethoxy-diphenylamine (DPA) in a cross-coupling reaction.1.68 g of 4,4′-dimethoxy-diphenylamine (2.08 g, 9.0 mmol), sodium t-butoxide (0.87 g, 9.0 mmol), and the catalyst bis (tri-tert-butylphosphine) palladium (0) (10 mg, 20 μmol) were well mixed in a 50 ml flask bottle. Then, 25 ml of dry toluene was added into the flask. The reaction flask was heated to 110 °C for one day. The solution color in the flask was observed from yellow to dark brown. The crude product was extracted from ethyl acetate and deionized water/HCl six times to remove extra impurities. Then, the target product DPA-C16 was separated from column chromatography, resulting in a yellow powder with a yield of 40 % less.

2.3. Preparation of freestanding DPA-C16/Ag/PMMA sensing materials

To prepare DPA-C16/Ag/PMMA sensing materials, the electrospinning precursor solution was prepared by dissolving DPA-C16, Ag NPs, and PMMA in DMF. PMMA (MW ~ 120,000 Da) was purchased from Sigma-Aldrich and used without further purification. DPA-C16 was added to the spinning solution at a concentration of 5.0 wt% relative to PMMA, while Ag NPs were incorporated at a concentration of 1.0 wt% relative to PMMA. The precursor solution was stirred at 80 °C for 3 h until the polymer was completely dissolved. The DPA-C16/Ag/PMMA nanofibers were fabricated using the electrospinning technique from the precursor solution mentioned above. The electrospinning device includes a syringe pump (KDS-100, KD Scientific Inc., USA), a high-voltage power supply (SC-PME50, Global Co. Ltd., Taiwan), and a grounded rotary collector with a diameter of 15.0 cm and a length of 15.0 cm (FES-COS, Falco Tech Enterprise Co. Ltd., Taiwan). The optimized electrospun parameters in the operation were an applied voltage of 10.0–25.0 kV, a working distance of 10.0 cm, a flow rate of 0.5 ml/h, a solution volume of 10 ml, and a receiving plate speed of 500 rpm.

2.4. Material characterization

For the morphology of various electrospun fibers, a field-emission scanning electron microscope (FE-SEM, model SU8010, Hitachi, Japan) was used for the observation. At least 100 fibers were counted to obtain fiber diameter distribution. The microstructures of Ag NPs were observed by using the transmission electron microscope (TEM, JEM-2100Plus, JEOL, Japan). The percentage distribution of particles' sizes was obtained from individual measurements of at least 100 particles. Ultraviolet–visible (UV–Vis) absorption spectra were measured by a UV–Vis spectrophotometer (UV-1900i, Shimadzu, Japan). The optical characteristics are explored through photoluminescence spectroscopy

with a 532 nm diode laser (LDH-PC-375, PicoQuant). The hydrophilicity of carbazole-based materials was evaluated using a water contact angle goniometer (100SB, Sindatek Instruments Co. Ltd).

2.5. Optical measurement of extinction spectrum

The VOCs were injected into a 4.5 cm by 4.0 cm by 4.0 cm quartz glass container to simulate the concentration of alcohol vapor. Measurements are taken at room temperature (25 °C) with a relative humidity range of 60 %. To prevent the interference of environmental humidity, the response time is defined as the extinction change value exceeding the extinction change maximum (ΔE_{max}) of blank (air). Namely, as the ΔE that is over the threshold of the $\Delta E_{max,\ air}$. In the beginning, the DPA-C16/Ag/PMMA sensing material was placed in the middle of the container. The target solvent with a specific concentration was injected into the quartz chamber and the extinction spectrum was measured every 30 s immediately. The extinction spectrum was measured by UV–Vis spectrophotometer from the wavelength 400 nm to 1000 nm. The maximum extinction change (ΔE) of the peak is determined as the sensitivity for a particular VOC. The absorption behavior of the sensing material results in a variety of extinction intensities. Therefore, the extinction change of the peak is defined by the extinction before and after the VOC sensing. The extinction formula is defined as follows:

$$\Delta E = E_t - E_{t_0} \quad (1)$$

where E_{t0} represents the extinction intensity of the peak before the VOCs detection and E_t represents the extinction intensity of the peak after the VOCs detection.

3. Results and discussion

Fig. 1 provides a comprehensive characterization of the synthesized Ag NPs. The TEM image demonstrates the morphology and dispersion of the nanoparticles, revealing well-dispersed, spherical Ag NPs with smooth surfaces as shown in Fig. 1(a). The Ag NPs size distribution is depicted in Fig. 1(b), showing a relatively narrow range around 11.4 ± 2.1 nm. Fig. 1(c) displays the UV–Vis absorption spectrum of the Ag NPs, where a distinct surface plasmon resonance (SPR) peak is observed around 420–450 nm. This SPR peak is characteristic of Ag NPs, confirming the successful synthesis and the collective oscillation of their surface electrons upon light excitation.

To utilize the SPR effect of Ag NPs, Ag NPs were dispersed in PMMA electrospinning precursor. The Ag/PMMA concentration in the precursor solution was controlled between 2.0 wt% and 10.0 wt% and employed electrospinning to fabricate sensing fibers, as illustrated in Fig. 2(a ~ d). The results indicate that increasing the PMMA concentration in the precursor solution raises the solution's surface tension, which subsequently reduces its stretching capability during electrospinning, resulting in thicker fiber diameters. The average fiber diameters were measured to be 45.0 ± 18.0, 168.0 ± 77.0, 407.0 ± 181.7, and 782.0 ± 209.1 nm for PMMA concentrations of 2.0, 5.0, 7.0, and 10.0 wt%, respectively, demonstrating a clear positive correlation between PMMA concentration and fiber diameter as shown in Fig. 2(e) and Table 1. At a PMMA concentration of 2.0 wt%, the fibers exhibit discontinuities, breakage, and beading, likely due to the insufficient polymer content required to form a stable and continuous fiber network during the electrospinning process (Fig. 2(a)). At 5.0 wt%, the fibers are more uniform and continuous, mitigating the discontinuities observed at lower concentrations (Fig. 2(b)). However, at concentrations of 7.0 wt% and 10.0 wt%, the fiber diameters increase significantly, and the electrospinning process becomes less stable, potentially leading to challenges in process control and compromising the sensing performance due to excessive fiber thickness. Based on these observations, a PMMA concentration of 5.0 wt% was selected for the preparation of the sensing film, as it offers an optimal balance between fiber continuity and

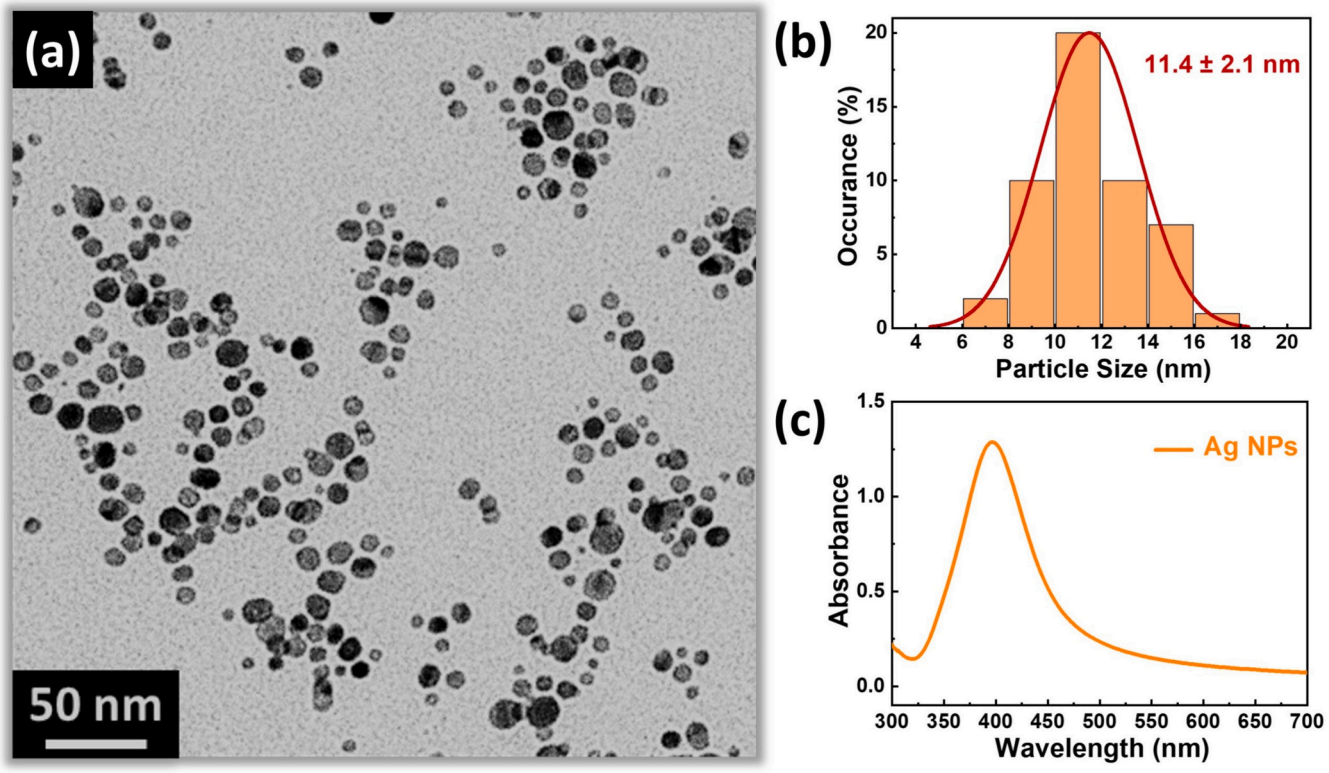

Fig. 1. (a) TEM image of Ag nanoparticles, showing their morphology and dispersion, and (b) the particle size distribution of Ag nanoparticles. (c) absorption spectrum of Ag nanoparticles.

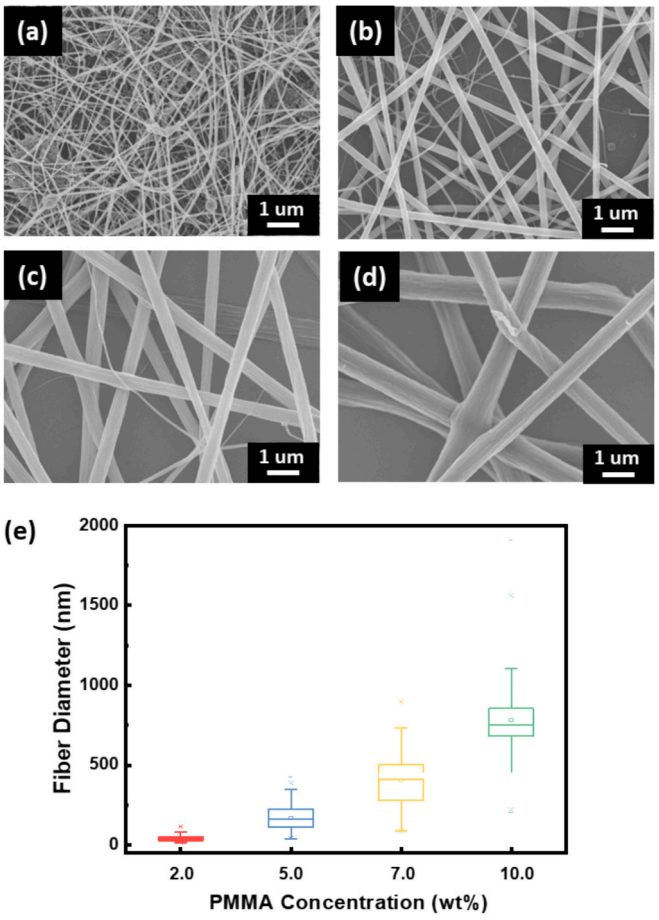

Fig. 2. FE-SEM morphology analysis of electrospun fibers Ag/PMMA with various PMMA concentrations in the precursor solution at (a) 2.0 wt%, (b) 5.0 wt%, (c) 7.0 wt%, and (d) 10.0 wt%. (e) Fiber diameter distribution diagram corresponding to PMMA concentrations ranging from 2.0 to 10.0 wt% in the precursor solution.

Table 1
The average fiber diameter for Ag/PMMA concentrations ranges from 2.0 to 10.0 wt% in the precursor solution.

PMMA Concentration (wt%)	Average Diameter (nm)
2.0	45.0 ± 18.0
5.0	166.0 ± 30.0
7.0	407.0 ± 181.7
10.0	782.0 ± 209.1

uniformity while maintaining manageable fiber diameters. This concentration also ensures consistent electrospinning process stability, contributing to the reliability and functionality of the sensing film.

By applying different applied voltages to the precursor solution containing Ag/PMMA at a PMMA concentration of 5.0 wt%, electrospinning was used to fabricate nanofibers with varying diameters, as shown in Fig. 3(a-d). When the applied voltage was 10.0 kV, the fiber diameter was measured to be 264.8 ± 67.6 nm. Increasing the voltage to 15.0 kV resulted in a reduction of the fiber diameter to 166.0 ± 30.0 nm. However, when the voltage was further increased to 20.0 kV, the fiber diameter rose to 222.5 ± 59.3 nm. At 25.0 kV, the fiber diameter increased to 254.4 ± 85.6 nm. The observed variations in fiber diameter and distribution are attributed to the influence of the applied voltage on the formation of the Taylor cone, which directly affects the stretching and thinning of the polymer jet during the electrospinning process. From the fiber diameter distribution chart shown in Fig. 3(e), it was

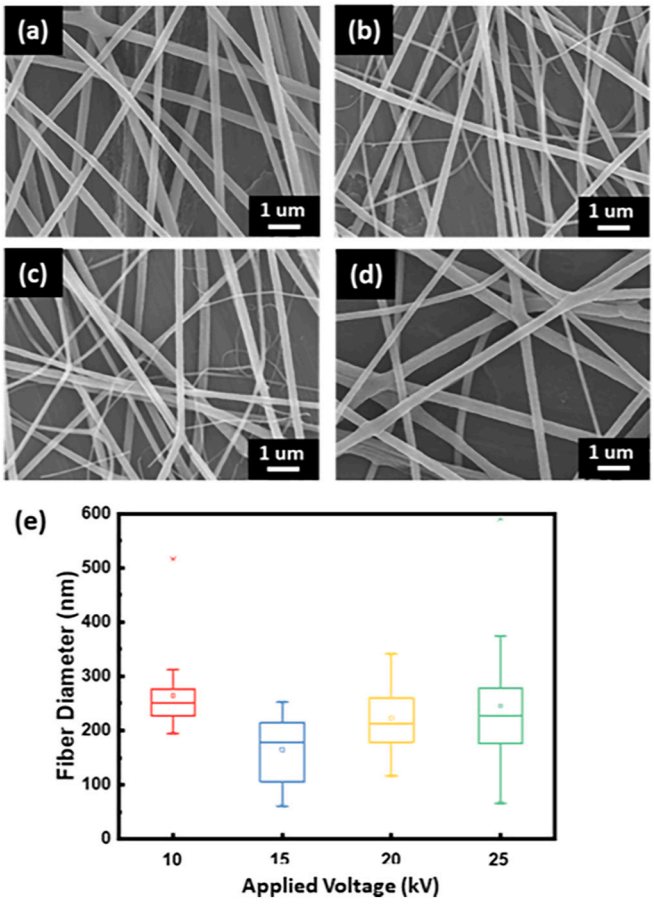

Fig. 3. FE-SEM morphological analysis of Ag/PMMA electrospun fibers applied at various applied voltages of (a) 10.0 kV, (b) 15.0 kV, (c) 20.0 kV, and (d) 25.0 kV. (e) Fiber diameter distribution chart for applied voltages ranging from 10.0 to 25.0 kV.

determined that the optimal voltage for producing the smallest fiber diameter was 15.0 kV. The fiber diameter distribution chart in Table 2 highlights the relationship between applied voltage and fiber diameter uniformity. Based on these findings, the optimal working voltage for achieving the smallest average fiber diameter with minimal variability was identified as 15.0 kV.

To evaluate the optical properties of DPA-C16, UV–Vis and PL measurements were conducted. The synthetic procedure to prepare the materials of carbazole alkylations can be found in the experimental section 2.2. Fig. S1 shows the characterization of UV–Vis absorption spectra and PL spectra of DPA-C16. The energy gap (Eg) derived from the absorption spectra was 3.28 eV. PL measurement was performed in chlorobenzene as a polar solvent and drop casted on glass slides. DPA-C16 displays an emission at approximately 530 nm. To confirm the successful synthesis of the DPA-C16 molecules, ^{1}H NMR spectra were recorded at room temperature, and referenced to residual DMSO solvent peak (Fig. S2). DPA-C16: ^{1}H NMR (600 MHz, $CDCl_3$, δ): 7.78–7.77 (d, 2H; CH), 7.58 (d, 2H; CH), 7.35 (d, 2H; CH), 4.25–4.00 (t, 2H; NCH_2),

Table 2
The average fiber diameter for Ag/PMMA applied voltages ranges from 10.0 to 25.0 kV.

Applied Voltage (kV)	Average Diameter (nm)
10.0	264.8 ± 67.6
15.0	166.0 ± 30.0
20.0	222.5 ± 59.3
25.0	254.4 ± 85.6

1.81(t, 2H; CH_2), 1.46–1.25(t, 26H; CH_2), 0.86(t, 3H; CH_3) ppm. DPA-C16: ^{1}H NMR (600 MHz, DMSO-d_6, δ): 7.77–7.74 (d, 2H; CH), 7.01–6.95 (m, 8H; CH), 6.89–6.84 (m, 10H; CH), 6.45–6.37 (dd, 2H; CH), 3.84–3.80 (t, 2H; NCH_2), 3.71 (s, 12H; CH_3), 1.49–1.45 (t, 2H; CH_2), 1.31–1.04 (m, 26H; CH_2), 0.74 (t, 3H; CH_3) ppm. DPA-C16, MALDI-TOF MS [M+] = 844.6, expected: 845. After the general purification procedure through thin layer chromatography (TLC) analysis and column chromatography (0–20 % EtOAc in hexanes gradient), the organic structure of DPA-C16, the product, is in good agreement with the theoretical chemical structure. The long alkyl hydrophobic chain on DPA-C16 promotes the compatibility between Ag NPs and electrospun fibers. The alkyl chain length on DPA-C16 is supposed to capture Ag NPs and the carbazole core is supposed to provide strong intermolecular interaction with PMMA electrospun fibers.

To investigate the effects of DPA-C16 on the morphology of electrospun fibers, we utilized FE-SEM to observe the surface morphology of the fibers as shown in Fig. 4. Compared to PMMA and Ag/PMMA fibers, which exhibit an average diameter of 172 ± 56 nm and 166 ± 30 nm (Fig. 4(a-d)), the DPA-C16/Ag/PMMA fibers demonstrate a significantly reduced average diameter of 106 ± 21 nm (Fig. 4(e,f)). This reduction in fiber diameter can be attributed to several potential factors. The addition of DPA-C16 could enhance the electrical conductivity or electrostatic charge density of the precursor solution, leading to greater stretching and thinning of the solution jet during the electrospinning process. As the solution jet experiences higher elongation forces under the electric field, the fibers formed are finer. Additionally, the carbazole groups in DPA-C16 may interact weakly with PMMA molecular chains, altering the rheological properties of the solution. This interaction could reduce the viscosity or modify the polymer chain entanglement, making the solution more prone to forming thinner jets during electrospinning. Furthermore, the improved distribution of charge carriers in the solution due to the presence of DPA-C16 could also result in more uniform electric field-induced stretching, which contributes to the formation of fibers with reduced diameters. These findings highlight the significant role of DPA-C16 in tailoring the fiber morphology by modifying the electrospinning dynamics and the solution properties.

Eliminating the impact of water vapor on alcohol gas sensors has always been a significant challenge. To investigate changes in the

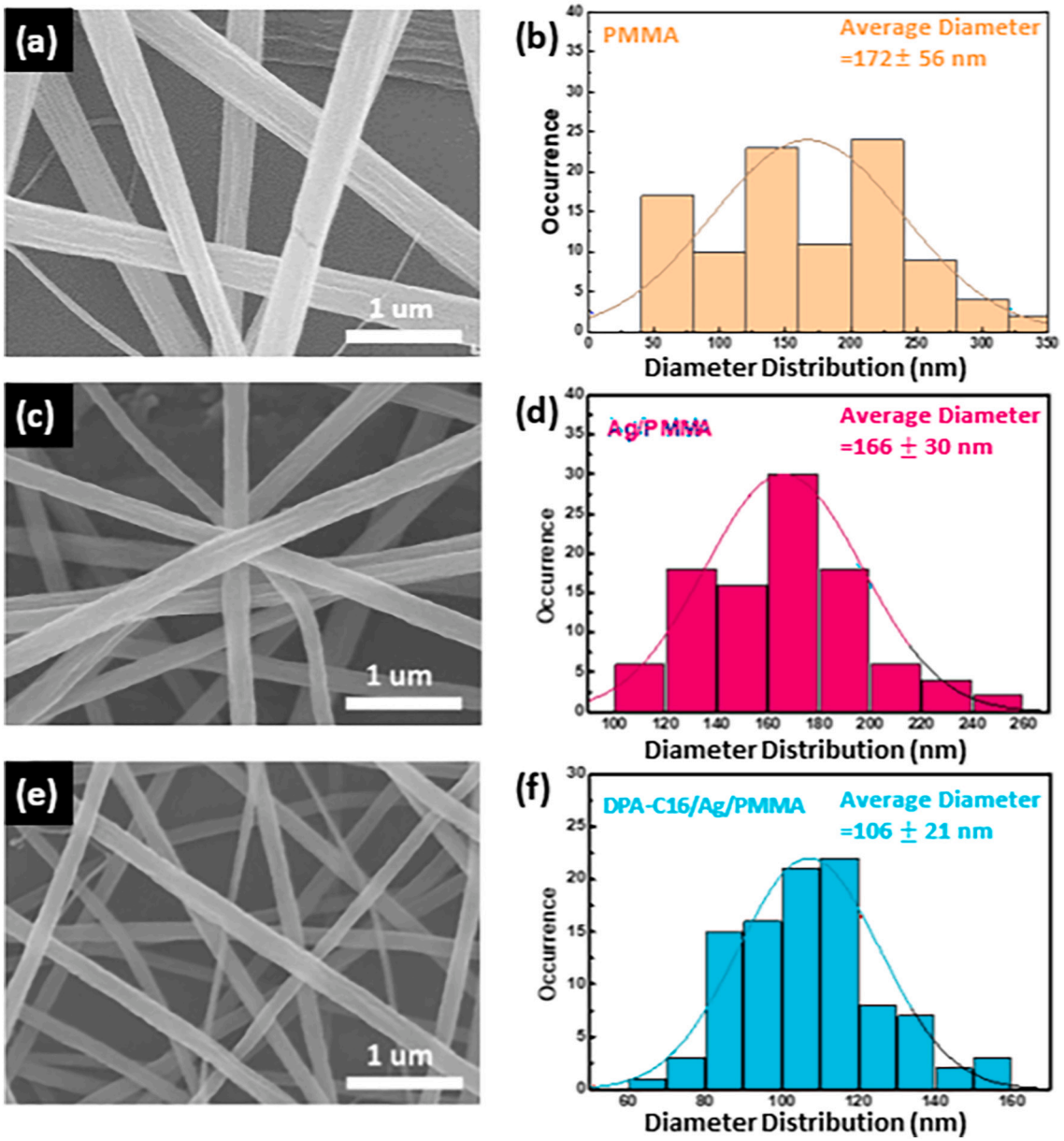

Fig. 4. FE-SEM surface morphology analysis and fiber diameter distribution charts for (a, b) PMMA, (c, d) Ag/PMMA, and (e, f) DPA-C16/Ag/PMMA.

hydrophilicity and hydrophobicity of fiber membranes after the addition of DPA-C16, we measured the water contact angle of the fiber membranes using a contact angle measurement instrument. As shown in Fig. 5(a) and 5(b), the water contact angles of PMMA and Ag/PMMA are relatively similar, measuring 118.2° and 117.6°, respectively. However, the water contact angle of DPA-C16/Ag/PMMA increases significantly to 133.4° (Fig. 5(c)). This substantial rise in the water contact angle indicates an enhancement in the hydrophobic properties of the fiber membrane. The increase in hydrophobicity can likely be attributed to the chemical structure of DPA-C16. Specifically, the carbazole groups in DPA-C16, which contain aromatic rings and nitrogen atoms, reduce the polarity of the fiber surface. Additionally, the long carbon chains in DPA-C16, consisting of sixteen carbon atoms, further amplify the hydrophobicity of the fiber membranes. This structural modification minimizes the influence of water vapor on the sensor's performance, making it more suitable for detecting alcohol gases in environments with varying humidity levels. The sensing performance of PMMA, Ag/PMMA and DPA-C16/Ag/PMMA was demonstrated in Fig. S3. The results clearly show that DPA-C16/Ag/PMMA exhibits the largest extinction change after exposure to isopropanol, demonstrating the synergistic enhancement arising from the combined effects of DPA-C16–assisted alcohol adsorption and Ag-induced plasmonic amplification.

Three types of alcohols (methanol, ethanol, and isopropanol) were selected to evaluate the gas sensing performance of the DPA-C16/Ag/PMMA nanofiber-based sensing material. The sensors were exposed to a wide range of vapor concentrations, from 10,000 ppm down to 50 ppm, to determine their detection limits and response characteristics. Extinction changes of DPA-C16/Ag/PMMA exposed to different concentrations of methanol, ethanol, and isopropanol are shown in Fig. 6. To further clarify the optical response behavior, Fig. S4 presents the extinction spectra of DPA-C16/Ag/PMMA fibers exposed to isopropanol vapor with concentrations ranging from 10,000 ppm to 50 ppm. A notable decrease in extinction intensity is observed in the 400–500 nm region, indicating strong optical interaction between the vapor molecules and the sensing film. The optical response parameter (ΔE) shown in Fig. 6 was calculated at 410 nm based on the extinction variation extracted from these spectra. The results showed that the DPA-C16/Ag/PMMA sensing material could produce a rapid response within 1 min for all three alcohols, demonstrating its capability for fast detection. Furthermore, the sensing response intensity increased significantly with the carbon chain length of the alcohol molecules, indicating higher sensitivity to alcohols with a greater number of carbon atoms. This phenomenon can be partly attributed to the solvent compatibility of carbazole, a key functional group in DPA-C16. Although carbazole is insoluble in water, it dissolves well in alcohols, which likely facilitates interactions between the alcohol molecules and the surface of the sensing material. These interactions may accelerate the collapse process of the fiber structure, thereby enhancing the sensing response intensity. Additionally, the carbazole groups in DPA-C16 might form weak hydrogen bonds or intermolecular interactions with the alcohol molecules, further enhancing the material's selective response to alcohol. Specifically, the experimental results revealed that the DPA-C16/Ag/PMMA sensing material exhibited more pronounced sensing performance for ethanol and isopropanol, indicating higher selectivity and sensitivity to alcohols with longer carbon chains. This could be attributed to the larger molecular size and stronger intermolecular forces of higher-carbon alcohols, which interact more effectively with the carbazole groups, thereby enhancing the sensing signals. Furthermore, the long alkyl chain of DPA-C16, consisting of 16 carbon atoms, might improve the hydrophobicity of the sensing material, further increasing its stability and selectivity in environments with

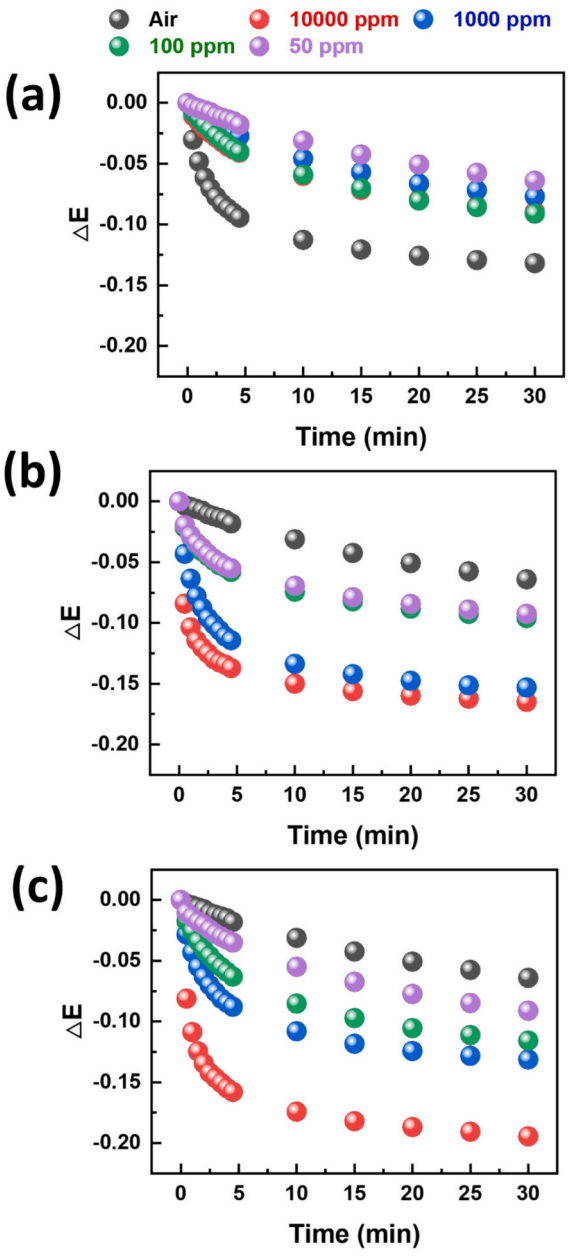

Fig. 6. Extinction changes of DPA-C16/Ag/PMMA exposed to different concentrations (in ppm) of (a) methanol, (b) ethanol, and (c) isopropanol.

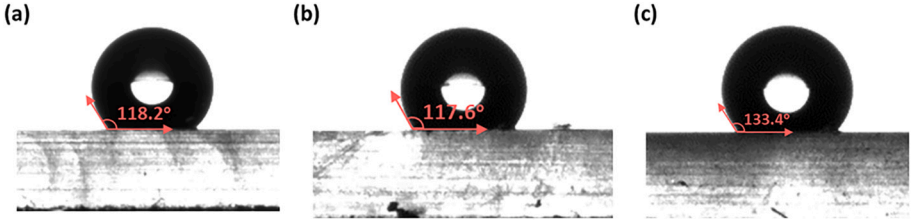

Fig. 5. Water contact angle analysis of sensing film made by various electrospun fibers, including (a) PMMA, (b) Ag/PMMA, and (c) DPA-C16/Ag/PMMA.

higher-carbon alcohols. The detection limit of the sensing material for all three alcohols was determined to be as low as 50 ppm, demonstrating excellent sensitivity to low-concentration alcohol vapors. Notably, in an isopropanol environment, the sensor was able to distinctly differentiate between different concentrations of isopropanol, highlighting its potential for precise detection of high-carbon alcohol vapors. This performance characteristic makes the DPA-C16/Ag/PMMA sensing material a highly promising candidate for alcohol gas sensors. The stability of the DPA-C16/Ag/PMMA sensing films was examined by storing the samples under ambient conditions for 5 and 15 days, followed by extinction change measurements (Fig. S5). The stability test was conducted by exposing the films to 10,000 ppm isopropanol vapor. The sensing response showed minimal decay, retaining 97.7 % of its initialΔE after 5 days and 94.4 % after 15 days, indicating that the material maintained stable performance after prolonged exposure to environmental humidity.

To investigate the sensing mechanism of DPA-C16/Ag/PMMA sensing films, we conducted a cross-sectional FE-SEM analysis of the DPA-C16/Ag/PMMA fibers before and after exposure to isopropanol (Fig. 7(a) and (b)). The results reveal a significant decrease in the thickness of the fiber film after exposure to isopropanol. This observation suggests that isopropanol molecules are either adsorbed onto or infiltrate the PMMA fibers, leading to a swelling effect. The swelling disrupts the stability of the three-dimensional (3D) fiber network, weakening the structural integrity and ultimately resulting in fiber collapse. This collapse of the fiber structure is a critical factor influencing the sensing performance of the film. Based on these findings, we propose a detailed sensing mechanism for the DPA-C16/Ag/PMMA sensing film for alcohols, as illustrated in Fig. 7(c). Initially, when the fibers are exposed to alcohol vapor, the high specific surface area of the nanofiber film and the compatibility between the solubility parameters of the alcohol molecules and the PMMA matrix promote the adsorption and penetration of alcohol molecules. In addition, the carbazole-based material, incorporated within the PMMA matrix, is known to be slightly soluble in ethanol, further enhancing its solvent uptake rate for alcohol vapors. [33,34] These interactions weaken the inter-fiber forces and facilitate the infiltration of alcohol molecules into the fiber structure. Swelling of polymer materials refers to the penetration of solvent molecules into the polymer matrix, leading to an increase in volume and alteration of internal morphology. Such solvent uptake and subsequent swelling can induce mechanical instabilities, including deformation or collapse of the polymer network, thereby influencing both the optical and mechanical behavior of the material. [35] As the alcohol molecules infiltrate the fiber matrix, the fibers undergo swelling due to the disruption of intermolecular interactions within the PMMA. This swelling causes a rearrangement of the 3D fiber network, destabilizing the structure. With continued exposure to alcohol molecules, excessive swelling further compromises the network's stability, ultimately causing the fibers to collapse completely. This collapse not only affects the physical structure of the film but also alters the optical properties of the sensing material. Specifically, the collapse of the fibers modifies the light transmission pathways within the sensing film, resulting in changes in its extinction capacity. These optical changes form the basis of the sensor's response, as variations in light extinction can be detected and correlated to the concentration of alcohol vapor present. The sensitivity of the sensing film to alcohol vapors is therefore directly linked to the fiber's ability to swell and collapse upon exposure. Furthermore, the selective response of the sensing film to different alcohols can also be explained by this mechanism. Higher-carbon alcohols, such as isopropanol, have stronger interactions with the fiber matrix due to their larger molecular size and stronger van der Waals forces. These interactions lead to more pronounced swelling and structural rearrangement, enhancing the film's sensitivity and selectivity to these alcohols. In contrast, smaller alcohol molecules like methanol induce less swelling and structural disruption, resulting in a weaker response.

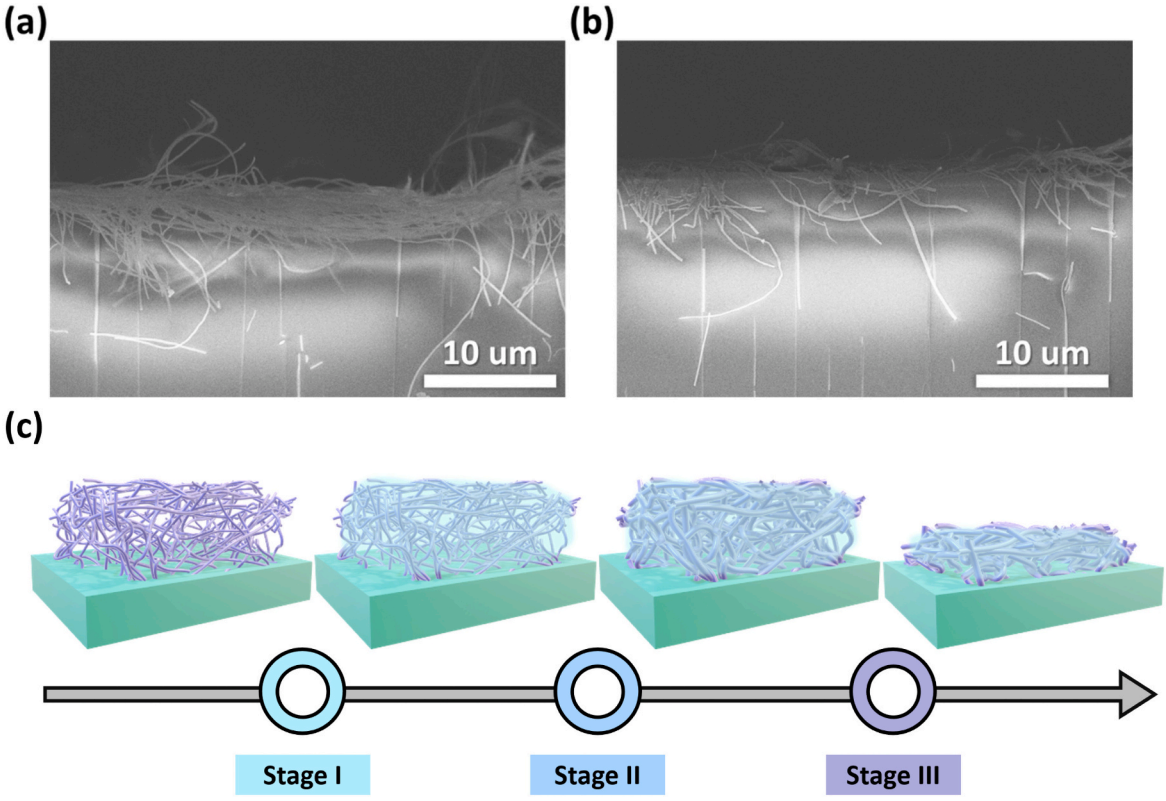

Fig. 7. Cross-sectional FE-SEM analysis of DPA-C16/Ag/PMMA fibers (a) before and (b) after exposure to isopropanol. (c) Schematic illustration of the sensing mechanism of the DPA-C16/Ag/PMMA sensing film.

4. Conclusion

In summary, the sensing mechanism of DPA-C16/Ag/PMMA electrospun nanofibers is primarily driven by the adsorption and infiltration of alcohol molecules into the fiber matrix, leading to fiber swelling, subsequent collapse of the 3D structure, and ultimately, changes in the optical properties of the electrospun film. Through an optimization process, the ideal conditions were determined to be a composition of 5.0 wt% Ag/PMMA and an applied voltage of 15.0 kV, which resulted in the formation of uniform, fine nanofibers with significantly improved optical characteristics and enhanced hydrophobicity, as evidenced by a high contact angle measurement of 133.4°. The fabricated DPA-C16/Ag/PMMA fibers demonstrated exceptional sensing performance, including a remarkably rapid response time of less than one minute and an impressive detection limit of 50 ppm for alcohol vapors. Notably, these fibers exhibited outstanding selectivity for isopropanol, which can be attributed to the pronounced fiber swelling and structural collapse induced upon alcohol adsorption. The results of this study strongly establish DPA-C16/Ag/PMMA electrospun nanofibers as highly efficient and selective gas-sensing materials, making them promising candidates for a wide range of industrial, environmental, and safety applications. Furthermore, this research paves the way for further refinement and optimization of the material, as well as its potential expansion into the detection of other volatile organic compounds.

CRediT authorship contribution statement

Tz-Feng Lin: Writing – original draft, Resources, Investigation. **Yin-Hsuan Chang:** Writing – original draft, Methodology, Investigation. **Ting-Hung Hsieh:** Investigation. **Shu-Chi Lu:** Investigation. **Ting-Han Lin:** Methodology, Investigation. **Hao-Yun Yu:** Investigation. **Ming-Chung Wu:** Writing – review & editing, Supervision, Methodology, Funding acquisition, Conceptualization.

Funding

The financial support from National Science and Technology Council, Taiwan (Project No. 111–2221-E-182-040-MY3, 113–2628-E-182-001-MY4, and 114–2923-E-182-001-MY3), and Chang Gung Memorial Hospital at Linkou (CMRPD2M0122, and BMRPC74) are highly appreciated. The authors expresses gratitude for the financial support provided by Chang Gung University (URRPD2Q0021, URRPD2Q0031 and URRPD2Q0041).

Declaration of competing interest

The authors declare the following financial interests/personal relationships which may be considered as potential competing interests: Ming-Chung Wu reports financial support was provided by Chang Gung University. Ming-Chung Wu reports financial support was provided by Linkou Chang Gung Memorial Hospital. Ming-Chung Wu reports financial support was provided by National Science and Technology Council, Taiwan. If there are other authors, they declare that they have no known competing financial interests or personal relationships that could have appeared to influence the work reported in this paper.

Acknowledgements

The authors appreciate Dr. Ming-Tao Lee (BL-13A1), Dr. Jeng-Lung Chen (BL-17C1) and Dr. Ting-Shan Chan (BL-01C1) at National Synchrotron Radiation Research Centre for helpful discussion and suggestions, and Mr. Y.-S. Chen at Instrumentation Centre of National Tsing Hua University for TEM analysis. The authors thank the Microscopy Center at Chang Gung University for technical assistance.

Appendix A. Supplementary data

Supplementary data to this article can be found online at https://doi.org/10.1016/j.surfcoat.2025.132883.

Data availability

Data will be made available on request.

References

[1] J. Lin, X. Feng, J. Huang, Y. Liu, Y. Xiao, Y. Li, Y. Min, B.Z. Tang, Biosens. Bioelectron. 267 (2025) 116799.
[2] E. Brobbin, P. Deluca, S. Coulton, C. Drummond, Alcohol Alcohol. 59 (2024) agad068.
[3] B. Bhagat, S.K. Gupta, D. Mandal, R. Bandyopadhyay, K. Mukherjee, Chemphyschem 25 (2024) e202300730.
[4] J.-C. Wang, H. Ma, W. Shi, W. Li, Z. Zhang, Y. Hou, W. Zhang, J. Chen, J. Environ. Chem. Eng. 12 (2024) 112698.
[5] G. Wu, H. Du, K. Pakravan, W. Kim, Y.L. Cha, M. Beidaghi, X. Zhang, X. Pan, D.-J. Kim, Carbon 216 (2024) 118565.
[6] X. Chen, J. Wang, J. Zhang, H. Lin, M. Tian, M. Li, Y. Tian, Chem. Eng. J. 486 (2024) 150204.
[7] J. Wang, S. Liu, Z. Chen, T. Shen, Y. Wang, R. Yin, H. Liu, C. Liu, C. Shen, J. Mater. Sci. Technol. 213 (2025) 213–222.
[8] Y. Zu, Z. Duan, Z. Yuan, Y. Jiang, H. Tai, J Mater Chem A 12 (2024) 27157–27179.
[9] M.-H. Jung, M. Kwak, J. Ahn, J.-Y. Song, H. Kang, H.-T. Jung, ACS Sensors 9 (2024) 217–227.
[10] N. Phukkaphan, C. Khunarak, T. Kerdcharoen, 2024 9th International STEM Education Conference (iSTEM-Ed), 2024, pp. 1–4.
[11] J. Shi, W. Tao, Y. Zhou, P. Zhang, G. Liang, Chem. Eng. J. 498 (2024) 155737.
[12] S.S. Gaikwad, A.S. Khune, N.N. Ingle, M.D. Shirsat, Sensors Actuators A Phys. 377 (2024) 115665.
[13] H. Selvi, I. Capan, R. Capan, Y. Acikbas, J. Mater. Sci. Mater. Electron. 35 (2024) 1268.
[14] M.M. Abutalib, Phys. B Condens. Matter 552 (2019) 19–29.
[15] D.L. Vu, T.-F. Lin, T.-H. Lin, M.-C. Wu, Polymers 12 (2020) 455.
[16] D.L. Vu, Y.-Y. Li, T.-H. Lin, M.-C. Wu, J. Taiwan Inst. Chem. Eng. 99 (2019) 250–257.
[17] S. Kassim, S.C. Padmanabhan, M.E. Pemble, Appl. Surf. Sci. 569 (2021) 151014.
[18] M.-C. Wu, C.-H. Lin, T.-H. Lin, S.-H. Chan, Y.-H. Chang, T.-F. Lin, Z. Zhou, K. Wang, C.-S. Lai, ACS Appl. Mater. Interfaces 11 (2019) 34454–34462.
[19] Y.-H. Chang, T.-H. Hsieh, K.-C. Hsiao, T.-H. Lin, K.-H. Hsu, M.-C. Wu, Polymers 15 (2023) 1833.
[20] T.-H. Lin, Y.-H. Chang, T.-H. Hsieh, Y.-C. Huang, M.-C. Wu, Polymers 15 (2023) 4318.
[21] M.-C. Wu, C.-K. Kao, T.-F. Lin, S.-H. Chan, S.-H. Chen, C.-H. Lin, Y.-C. Huang, Z. Zhou, K. Wang, C.-S. Lai, Sensors Actuators B Chem. 309 (2020) 127760.
[22] C.V. Sudheep, A. Verma, P. Jasrotia, J.J.L. Hmar, R. Gupta, A.S. Verma, Jyoti, A. Kumar, T. Kumar, Res Chem. 7 (2024) 101255.
[23] X. Guo, Y. Sun, X. Sun, J. Li, J. Wu, Y. Shi, L. Pan, Macromol. Rapid Commun. 45 (2024) 2300246.
[24] Y. Zhu, M. Wei, X. Ma, H. Ma, R. Chen, H. Zhang, X. Wang, J. Ji, M. Xue, Macromol. Rapid Commun. 45 (2024) 2400037.
[25] H. Roh, D.-H. Kim, Y. Cho, Y.-M. Jo, J.A. del Alamo, H.J. Kulik, M. Dincă, A. Gumyusenge, Adv. Mater. 36 (2024) 2312382.
[26] J. Shao, H. Huang, X. Liu, X. Lan, S. Ren, W. Liu, Microchem. J. 209 (2025) 112824.
[27] S. Lee, S.-H. Kim, S. Lee, Y. Lee, Y.S. Lee, K.-H. Yang, K.-K. Wang, W.-S. Han, Dyes Pigments 194 (2021) 109613.
[28] H. Ramezanipour Penchah, A. Ghaemi, P. Valipour, M. Shahbazi, Sensors Int. 4 (2023) 100249.
[29] X.-Y. Luo, Y.-L. Lu, Z. Wang, M. Pan, ChemPhotoChem 7 (2023) e202200200.
[30] J. Qian, Q. Lu, F. Xu, L. Chen, J. Xia, J. Hazard. Mater. 410 (2021) 124544.
[31] C. Immanuel David, G. Prabakaran, A. Karuppasamy, J.C. Veetil, R.S. Kumar, A. I. Almansour, K. Perumal, C. Ramalingan, R. Nandhakumar, J. Photochem. Photobiol. A Chem. 425 (2022) 113693.
[32] N.C. Kekec, F.E. Kanik, Y.A. Udum, C.G. Hizliates, Y. Ergun, L. Toppare, Sensors Actuators B Chem. 193 (2014) 306–314.
[33] L.B. Salam, M.O. Ilori, O.O. Amund, 3 Biotech 7 (2017) 111.
[34] D. Shah, M. Patel, A. Vyas, A. Patel, Arch. Pharm. 358 (2025) e70096.
[35] F.K. Metze, S. Sant, Z. Meng, H.-A. Klok, K. Kaur, Langmuir 39 (2023) 3546–3557.